Journal of Environmental Chemical Engineering 13 (2025) 120445

Contents lists available at ScienceDirect

Journal of Environmental Chemical Engineering

journal homepage: www.elsevier.com/locate/jece

Fabrication of kappa carrageenan-cellulose nanofiber/graphene oxide composite membrane for water purification

Lilyan Alsaka [a], Ali Altaee [a,*], Armaghan Moghaddam [b], Hossein Ali Khonakdar [b], Maryam AL-Ejji [c], Alaa H. Hawari [d], Faris Hamdi [a,e], Yahia Aedan [a], Abdulmajeed Al Askar [a,f]

[a] Centre for Green Technology, School of Civil and Environmental Engineering, University of Technology Sydney, 15 Broadway, Sydney, NSW 2007, Australia
[b] Faculty of Polymer Processing, Iran Polymer and Petrochemical Institute (IPPI), Tehran 14965-115, Iran
[c] Center of Advanced Materials, Qatar University, PO Box 2713, Doha, Qatar
[d] Department of Civil and Environmental Engineering, College of Engineering, Qatar University, PO Box 2713, Doha, Qatar
[e] Department of Civil and Architectural Engineering, College of Engineering and Computer Sciences, Jazan University, PO Box 114, Jazan 45142, Saudi Arabia
[f] Department of Chemical Engineering, College of Engineering and Computer Sciences, Jazan University, Jazan 45142, Saudi Arabia

ARTICLE INFO

Keywords:
Hydrogel membrane
Filtration
Desalination
Seawater
Kappa-carrageenan

ABSTRACT

This research investigates the synthesis, optimization, and assessment of kappa-carrageenan (kC)-cellulose nanofiber (CNF)/glutaraldehyde (GA)coated with graphene oxide (GO) for seawater treatment. The kC hydrogel was crosslinked with GA to enhance mechanical strength and adsorption efficiency. The SEM, EDX, and FT-IR analyses revealed a well-defined porous structure, uniform coating, and significant functional groups. Based on swelling behavior, the average molecular weight between crosslinks (Mc) was calculated to evaluate network tightness. The addition of CNF increased the stiffness of the membranes and affected the internal network, resulting in reduced swelling, smaller Mc values, and decreased average pore radius. While this structural tightening reduced the water flux, it improved salt rejection. In the first stage, ion removal ranged from 85 % to 92.7 % but it decreased from 79.6 % to 82.3 % in the second stage, resulting in freshwater with a concentration of 692 mg/L. Reusability studies showed that the hydrogel maintained nearly consistent performance in multiple cycles, with a drop in rejection of 19 % sodium chloride and 14 % magnesium sulfate in 3rd cycle, while water flux declined by 25.8 % and 17.6 % for sodium chloride and magnesium sulfate. Antifouling experiments conducted in multiple cycles at a 90 % recovery rate found 89.7 % water flux recovered after DI water cleaning in 1st cycle and 82.5 % in 3rd cycle. The kC-CNF/GO-GA hydrogel provides a solution for the treatment of seawater that is not only cost-effective but also sustainable and environmentally friendly.

1. Introduction

Water shortage and pollution are significant global challenges that threaten people's health and the environment's sustainability. The demand for water purification techniques has become more critical than ever because of the increasing population, industry water demands, and increased agricultural activities. Despite their effectiveness, conventional water purification methods consume high energy to be sustainable. These challenges make hydrogel membranes, particularly those fabricated from natural and renewable resources, a potential technology for water purification.

Cellulose nanofibrils (CNFs) offer advantages such as their high length-to-diameter ratio, excellent tensile strength, large surface area, and ease of mixing with other substances. Because they are one-dimensional, they are perfect for making hybrid nanomaterials for water purification. When crosslinked, they make two-dimensional films, three-dimensional hydrogels, or aerogels. The carboxyl groups on CNF are essential for building a solid network, while electronegative oxygen and hydrogen atoms can make a weak bond, which is the essence of hydrogen bonding [46]. CNF-based products found applications in water treatment and purification. New research has focused on making, changing, and using CNF in water treatment that addresses environmental problems [29,37]. For example, polyamidoxime-nanocellulose (PAO-CNF) hydrogels worked well to remove uranium from seawater, reaching 6.6 mg-U/g [15]. When CNF was added to starch-g-poly (acrylic acid) hydrogels, the super-adsorbent products adsorbed Cu up

* Corresponding author.
E-mail address: ali.altaee@uts.edu.au (A. Altaee).

https://doi.org/10.1016/j.jece.2025.120445
Received 22 September 2025; Received in revised form 20 November 2025; Accepted 22 November 2025
Available online 24 November 2025

to 0.957 g/g in a 0.6 g/L solution. As the Cu) concentration went up, so did the adsorption, particularly in an acidic environment of pH 1–2 [5].

Another natural polysaccharide material extracted from red seaweed and used for water purification is kappa carrageenan (kC). It has been studied extensively for its ability to gel and be compatible with living beings. Its special chemical structure, with sulfate groups and high molecular weight, makes it an excellent material for making hydrogels that can hold and absorb water [33]. Notably, the composite hydrogel from combining kC with CNFs exhibited exceptional mechanical strength, stability, and adsorption capacity.

In hydrogel formation, kC and CNF are particularly advantageous for desalination and water purification. The combination of kC with CNF has unique properties, including kC's ionic nature and swelling ability that facilitates the elimination of contaminants, while CNF provides structural reinforcement, enhancing the hydrogel's durability and reusability. Crosslinking CNF with acrylic acid (AA) produced cellulose nanofiber aerogel that was able to uptake about 40.01 mg/g Cu(II) and 130.36 mg/g Pb(II) [36]. The kC/cellulose hydrogel demonstrated a maximum adsorption capacity of 486 ± 28.5 mg/g for Pb^{2+}. It maintained over 79 % Pb^{2+} removal efficiency after eight adsorption-desorption cycles [18]. A study by Štefelová for dyes removal from wastewater by CNF adsorbent achieved 99.8 % of methylene blue at 40 mg/L concentration, as well as crystal violet and Congo red [35].

Wang et al. [38], for example, fabricated a 3D network of cellulose/graphene oxide (CG) porous composites to make aerogels capable of adsorbing 421.9 mg/g of methylene blue and 163.4 mg/g of tetracycline [38]. A new kC-g-PHEAA hydrogel with FeO_2 nanoparticles was able to absorb methylene blue (MB), rhodamine 6 G (R6G), Cu(II), and Hg(II) [23]. kC-GO was used to coat the NF membrane to improve its fouling resistance and achieved 95.73 % water flux recovery [42]. Carrageenan and adjusted Carrageenan and nanocellulose-adjusted carrageenan beads were able to effectively remove Cu(II), Pb(II), Ca(II), Mg(II), and Fe(II) ions [3]. A GO-kC/SA gel, synthesized by calcium hardening, exhibited improved mechanical strength. The gel exhibited maximum adsorption capacities of 272.18 mg/g for Ciprofloxacin (CIP) and 197.39 mg/g for Ofloxacin (OFL), with an adsorption capacity of 83.99 mg/g for simulated OFL wastewater (200 mg/L) in a fixed-bed column system [44].

In this study, a glutaraldehyde (GA) crosslinked kC-CNF/GO composite hydrogel membrane was fabricated for seawater desalination. Initially, kC and CNF were crosslinked with GA to produce a hydrogel base layer that was coated with GO to enhance the rejection and antifouling characteristics of the kC-CNF/GO-GA composite membrane. The composite hydrogel membrane was investigated for i) the kC-CNF/GO-GA composite hydrogel efficiency to reject divalent and monovalent ions, ii) the effect of CNF on the water flux and ion rejection capabilities, and iii) the feasibility of seawater desalination by the kC-CNF/GO-GA composite hydrogel membrane. The performance and reusability of the kC-CNF/GO-GA composite hydrogel membrane were investigated in multiple cycles for seawater treatment as a sustainable desalination method.

2. Materials and methods

2.1. Materials

The following materials were used in the research: the sulphated plant polysaccharide (kappa carrageenan kC), glutaraldehyde solution (GA), and graphene oxide (GO) were acquired from Sigma-Aldrich in Australia, while cellulose nanofiber (CNF) was acquired from Nanografi Company in Turkey. For the rejection and adsorption studies, analytical grade chemicals such as magnesium sulphate ($MgSO_4$) 2 g/L, copper sulphate ($CuSO_4$) 2 g/L, and sodium chloride (NaCl) 2 g/L were procured from Sigma-Aldrich in Australia. Seawater was collected from a science lab at the University of Technology Sydney (Table 1). The real seawater samples were collected from the beach area in Sydney, Australia.

Table 1
Properties of seawater used in the filtration experiments.

Parameter	Seawater
pH	6.4
Conductivity	52 ± 2 ms/cm
Total Dissolved Solids	34788 ± 100 mg/L
Turbidity	0.22 ± 1 NTU
Na^+	10933 ± 5 mg/L
K^+	383 ± 2 mg/L
Mg^{2+}	1303 ± 5 mg/L
Ca^{2+}	413 ± 2 mg/L
Cl^-	19592 ± 5 mg/L
Si^{4+}	0.151 ± 0. 1 mg/L
Cu^{2+}	0.021 ± 0. 1 mg/L
Li^+	0.188 ± 0.1 mg/L
B^{3-}	5 ± 0.1 mg/L
F^-	1.05 ± 0.01 mg/L
S^{2+}	914 ± 0.01 mg/L
Ba^{2+}	0.011 ± 0.01 mg/L
Br^-	64 ± 2 mg/L

2.2. Synthesis of kC-CNF/GO-GA Hydrogel

The fabrication of the composite hydrogel consisted of the preparation of the base layer of kC-CNF/GA hydrogel coated with a thin layer of GO/GA to ensure the uniformity and structural stability of the membrane (Fig. 1a). First, a 3 %kC hydrogel was prepared by dissolving kC powder in deionized (DI) water, heating the mixture to 60–80°C, and stirring for 3 h at 800 rpm. Concurrently, a CNF hydrogel is created by dissolving 1–2.5 % CNF in DI water and using a hot water bath with sonication for 4–6 h. The kC and CNF were mixed for 1 h with 2 %GA to form a uniform spreadable hydrogel blend. Then, a GO/GA solution was prepared by sonicating 12.5 mg of GO in 250 mL DI water at 45°C for 12 h, mixed with a 2 %GA at a 2:1 ratio, and the final solution was mixed at 600 rpm for 2 h. To prepare the composite hydrogel membrane, the kC-CNF/GA hydrogel was packed in a filtration column, then 2.7 mL of GO-GA solution was added on top of the hydrogel at 0.5 bar for 2 h to produce a uniform 2 mm thick coating over the hydrogel membrane of 0.0013 m^2 active filtration area. It is noteworthy that excessive pressure could cause membrane defects and an uneven coating layer [42].

Fig. 1b illustrates the bonding techniques to create a stable structure in the kC-CNF/GA hydrogel with a thin GO/GA coating layer. The GA crosslinker promotes the formation of the following bonds: ether bonds (R–O–R′), acetal bonds (R–CH(OR')₂), and ester bonds (R–COO–R′). Ether bonds (R–O–R′) are formed when GA interacts with hydroxyl groups (-OH) on kC and CNF via a ring-opening mechanism, resulting in a stable internal matrix. Acetal linkages (R–CH(OR')₂) enhance structural integrity and stiffness since GA interlinks kC and CNF molecules via their hydroxyl groups. The GO coating is firmly bonded by ester linkages (R–COO–R′) established between carboxyl groups (-COOH) on GO and hydroxyl groups in the hydrogel, guaranteeing robust adhesion and a cohesive multilayer architecture. The amalgamation of ether, acetal, and ester linkages produces a highly crosslinked network that improves the mechanical stability, surface area, and structural integrity of the hydrogel. The characterization of kC-CNF/GO-GA hydrogel is in Table S1 (Supplementary Materials). Table 2 shows the hydrogel membranes used in the experiments for seawater desalination.

3. Hydrogel performance efficiency

3.1. Flux evaluation and rejection

The kC-(1–2.5)%CNF/GA hydrogel was cast on a lint support layer in a dead-end filtration column of 25 cm long and 0.0013 m^2 effective membrane area. After casting, the hydrogel was left to settle for

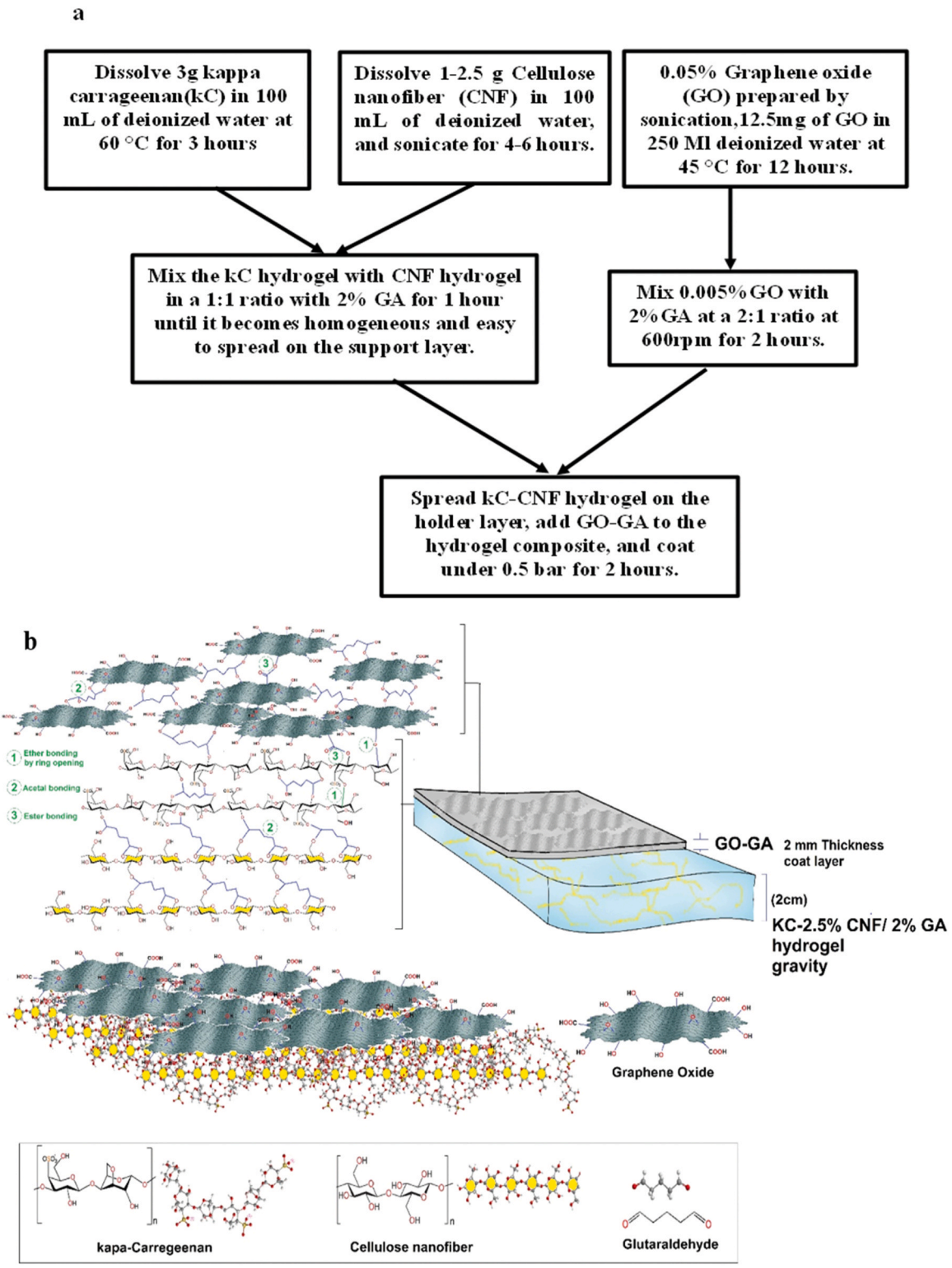

Fig. 1. Hydrogel preparation a) Hydrogel formation process a) Hydrogel formation process, b) Synthesis and structural Composition of kC-CNF/GO-GA (M_1, $M_{1.5}$, M_2, and $M_{2.5}$) hydrogel and molecular interactions within the hydrogel Network.

10–15 min; then, a 2 mm layer of the 0.05 %GO-2 %GA solution was added under 0.5 bar pressure for 2 h. Pure water flux (J) was evaluated using DI water feed according to Eq. 1:

$$J = \frac{V}{A * t} \tag{1}$$

where V is the permeate volume in m^3 over time t (hour), and A represents the effective surface area of the hydrogel (m^2). The salt rejection studies utilized solutions of 2 g/L $MgSO_4$ and NaCl in separate experiments. The ion rejection rate ($\%R$) was calculated from Eq. 2:

$$R(\%) = (1 - \frac{Cp}{Cf}) * 100 \tag{2}$$

In salt rejection studies, permeate concentration (Cp) and feed

Table 2
Composition of hydrogel membranes used in seawater desalination.

Hydrogel membranes	KC (g/100 mL)	CNF (g/100 mL)	GO (mg/250 mL)	GA (mL/100 mL)	Hydrogel composition
M_1	3	1	12.5	2	3 %KC-1 % CNF/0.05 % GO-2 %GA
$M_{1.5}$	3	1.5	12.5	2	3 %KC-1.5 % CNF/0.05 % GO-2 %GA
M_2	3	2	12.5	2	3 %KC-2 % CNF/0.05 % GO-2 %GA
$M_{2.5}$	3	2.5	12.5	2	3 %KC-2.5 % CNF/0.05 % GO-2 %GA

concentration (*Cf*) were quantified using ICP-MS (inductively coupled plasma-mass spectrometry). All experiments were conducted in triplicate, and results were presented with error bars.

3.2. Antifouling study for hydrogel

Antifouling experiments demonstrate the composite hydrogel's propensity to fouling. The experiments quantify the water flow before and after exposure to fouling materials to assess the hydrogel's capability to restore its filtering performance after cleaning. The baseline experiment first measured pure water flow (*J*1) for DI water. Afterward, the water flux (*Jf*) of the hydrogel filtering seawater was recorded. The hydrogel was rinsed with DI water at the end of this experiment, and the pure water flux (*J*2) was measured again. Water flux decline (DR%) and irreversible fouling (IFR%) were quantified in Eqs. 4 and 5 as follows:

$$FRR(\%) = \left(\frac{J2}{J1}\right) \times 100 \tag{3}$$

$$DR(\%) = \left(1 - \frac{Jf}{J1}\right) \times 100 \tag{4}$$

$$IFR(\%) = \left(1 - \frac{J2}{J1}\right) \times 100 \tag{5}$$

The water flux recovery (%FRR) reflects the antifouling effectiveness of the hydrogel in restoring the water flux after cleaning with DI water Eq. 3. The IFR represents irreversible fouling that was not removed after cleaning.

3.3. Methodology for analyzing the hydrogel properties

Small pieces (2.5 L×2.5 W×2D cm) of the membrane were cut and soaked in distilled water for 15 h to measure the hydrogel membrane's porosity. The wet membrane was weighed after carefully blotting excess water, and *weight1* was recorded. The samples were then dried in an oven at 60°C for 6 h and weighed again (*weight2*). Then, porosity (%) was calculated (Eq. 6):

$$P\% = \left(\frac{weight1 - weight2}{A * l * \rho}\right) \tag{6}$$

Eq. 7 calculates the hydrogel membrane's average pore radius size (rm) using the membrane porosity and pure water flux through the membrane. ΔP is the operation pressure, p is the membrane porosity, l and A are the thickness and effective membrane area, and Q is the volume of pure water flux per time (m^3/s)

$$rm = \sqrt{\frac{(2.9 - 1.75p) \times (8 \times lQ\eta)}{(p \times A \times \Delta P)}} \tag{7}$$

Water uptake (*Wu*) of the hydrogel was quantified by cutting a pre-dried hydrogel into small pieces of 2 × 2 × 1 cm. Following a drying period of 6 h at 105°C, the dry weight (*W*dry) was recorded. The segments were then immersed in distilled water for 24 h, and the wet weight (*W*wet) was documented after the removal of surplus water by blotting. *Wu* was determined from Eq. 8.

$$Wu = \left(\frac{Wwet - Wdry}{Wdry}\right) \times 100 \tag{8}$$

Eq. 9 calculates the swelling degree (*SD*) by recording the starting and final weights after immersing the hydrogel samples in DI water and (0.5–2.5 g/L) NaCl solutions for 2 h.

$$SD = \frac{(Wfinal - Winitial)}{Winitial} \times 100 \tag{9}$$

kC-CNF/GA hydrogels, with different CNF concentrations, were tested for deswelling. Hydrogels pre-swollen in water for 24 h were dried at 60°C, with weights declining every 30 min. Deswelling (*DS*) was calculated using Eq. 10, where *Wswollen* is the swollen hydrogel weight and *Wdry* is the weight after 30 min of oven drying (Eq. 10).

$$DS = \left(\frac{Wdry}{Wswollen}\right) \times 100 \tag{10}$$

To calculate the average molecular weight between crosslinks, the Flory-Rehner equation (without Gaussian chain correction) for hydrogels in water was used [7] as follows:

$$\frac{1}{M_C} = -\frac{\rho_P}{V_1} \cdot \frac{\ln(1-\nu_2) + \nu_2 + X\nu_2^2}{\nu_2^{\frac{1}{3}} - \frac{\nu_2}{2}} \tag{11}$$

where M_C represents the average molecular weight between crosslinks (g/mol), ρ_P represents the density of dry polymer constituents, V_1 represents the molar volume of the solvent (for water: 18.01 cm^3/mol), and X represents the Flory–Huggins polymer–solvent interaction parameter (dimensionless). In addition, ν_2 represents volume fraction of polymer in the swollen hydrogel and was calculated by Eq. 12 [12]:

$$\nu_2 = \frac{1}{1 + SD.\frac{\rho_P}{\rho_S}} \tag{12}$$

In Eq. 12, SD represents the swelling degree, ρ_p represents the density of dry polymer constituents, and ρ_S represents the density of solvent (water = 1.00 g/cm^3).

3.4. Adsorption-desorption performance analysis

Adsorption-desorption experiments were conducted on the best-performing $M_{2.5}$ hydrogel membrane used in the multiple filtration cycles for seawater desalination. The experiment on the adsorption capability of Na^+ and Mg^{2+} was carried out using a thermostatic shaker at a temperature of 25ºC, a pH of 6.5, and a rotational speed of 150 revolutions per minute (rpm) over five hours. During the experiment, a solid-to-liquid ratio of 2 g/L was used to combine NaCl and $MgSO_4$. To achieve the separation performance of the $M_{2.5}$, centrifugation at 10000 rpm for 10 min was performed after the adsorption tests. ICP analysis was used to measure the concentration of ions in the filtration samples, and Eq. 13 was used to compute the adsorption capacity in mg/g.

$$Adsorption\ capacity\left(\frac{mg}{g}\right) = (Ci - Cf) \times \frac{V}{W} \tag{13}$$

In Eq. 13, *Ci* is the ion concentration in mg/L, *Cf* is the residual ion concentration at equilibrium in mg/L, *V* is the solution volume in L, and *W* is the hydrogel sample weight in grams. After adsorption, desorption experiments were conducted by introducing 30 mL of 0.1 M hydrochloric acid (HCl) of pH 1.5 into vials containing 20 g of $M_{2.5}$ hydrogel. The desorption experiments were performed in a shaker at 25 °C, stirring

at 150 rpm for 3 h. Subsequently, the $M_{2.5}$ materials were separated by centrifugation at 10000 rpm for 10 min. Desorption capacity ($mg \cdot g^{-1}$) was calculated according to Eq. 14.

$$Desorption\left(\frac{mg}{g}\right) = \frac{(CR * V)}{Wgel} \quad (14)$$

CR represents the residual concentration of ions (mg/L), *V* is the volume of the HCl solution in Liters (L), and Wgel is the weight of the hydrogel in g.

4. Results

4.1. Rheology and zeta potential of hydrogel composites

Fig. 2a shows the rheological behavior of 3 %kC hydrogel, 2.5 %CNF hydrogel, and the $M_{2.5}$ hydrogel membrane. At a shear rate of 0.1 s^{-1}, 3 %kC demonstrates the highest viscosity of 2.68*10⁶ mPa·s and shear stress 268 Pa, while 2.5 %CNF starts with a viscosity of 1.21*10⁶ mPa·s and a shear stress of 120.87 Pa. The $M_{2.5}$ started with a low viscosity of 989,970 mPa·s and a shear stress of 99.01 Pa. With an increase in shear rate, all materials exhibited shear-thinning behaviour. For 3 %kC, the viscosity decreased to 9180 mPa·s at a shear rate of 100 s^{-1}, with a shear stress of 919.85 Pa. For 2.5 %CNF, the viscosity decreased steadily, reaching 12987 mPa·s at 100 s^{-1}, while the shear stress increased to 1300 Pa. The $M_{2.5}$ composite followed a similar shear-thinning behavior, with its viscosity decreasing to 8564.9 mPa·s at 100 s^{-1} and its shear stress increasing to 856.8 Pa. The attribute that the composite behaves in an intermediate manner between the kC and CNF materials indicates that it can maintain a balance between fluidity and mechanical strength. On account of this, it is appropriate for applications that need structural integrity and shear resistance. Rheological analysis figure S4 (Supplementary material) showed that increasing CNF concentration from M_1 to $M_{2.5}$ significantly enhanced viscosity and shear stress, indicating stronger network formation due to hydrogen bonding and fibril entanglement. $M_{2.5}$ exhibited the highest viscosity (9.89×10^5 mPa·s) and shear resistance, reflecting optimal reinforcement within the kC–GA matrix. All samples demonstrated shear-thinning behavior, confirming pseudoplasticity. These findings highlight CNF's role in enhancing mechanical stability and viscoelastic strength by densifying the network and improving polymer chain interactions. The M2.5 hydrogel membrane exhibits outstanding rheological properties suitable for water purification. It can retain a dense filtering matrix due to its shear-thinning properties, facilitating adequate water circulation at higher speeds and reducing the likelihood of accumulation.

Fig. 2b illustrates the zeta potential of various kC, CNF, and M_1 to $M_{2.5}$ hydrogel membranes. The pure kC, with a zeta potential of −41.4 mV ± −2.1, displays moderate colloidal stability, vital for contaminant adsorption. In contrast, pure CNF shows the highest stability with a zeta potential of −58.2 mV ± −2.9, showing enhanced electrostatic repulsion that facilitates the adsorption of positively charged ions, including heavy metals [20]. As CNF concentration increases in the kC matrix, the zeta potential becomes more negative, improving the material's ability to interact with charged ions and pollutants. For example, the $M_{2.5}$ hydrogel, with a zeta potential of −49.2 mV ± −2.5, shows significantly enhanced stability, attracting and entrapping charged pollutants [25]. The zeta potential plays a significant role in influencing electrostatic interactions with pollutants, especially due to the sulfate groups in kC and carboxyl groups in CNF, which enhance the adsorption of positively charged impurities via electrostatic attraction [2]. GA crosslinking stabilizes the hydrogel's structure without substantially reducing the zeta potential, assuring long-term effectiveness in water purification [11]. Further, a highly

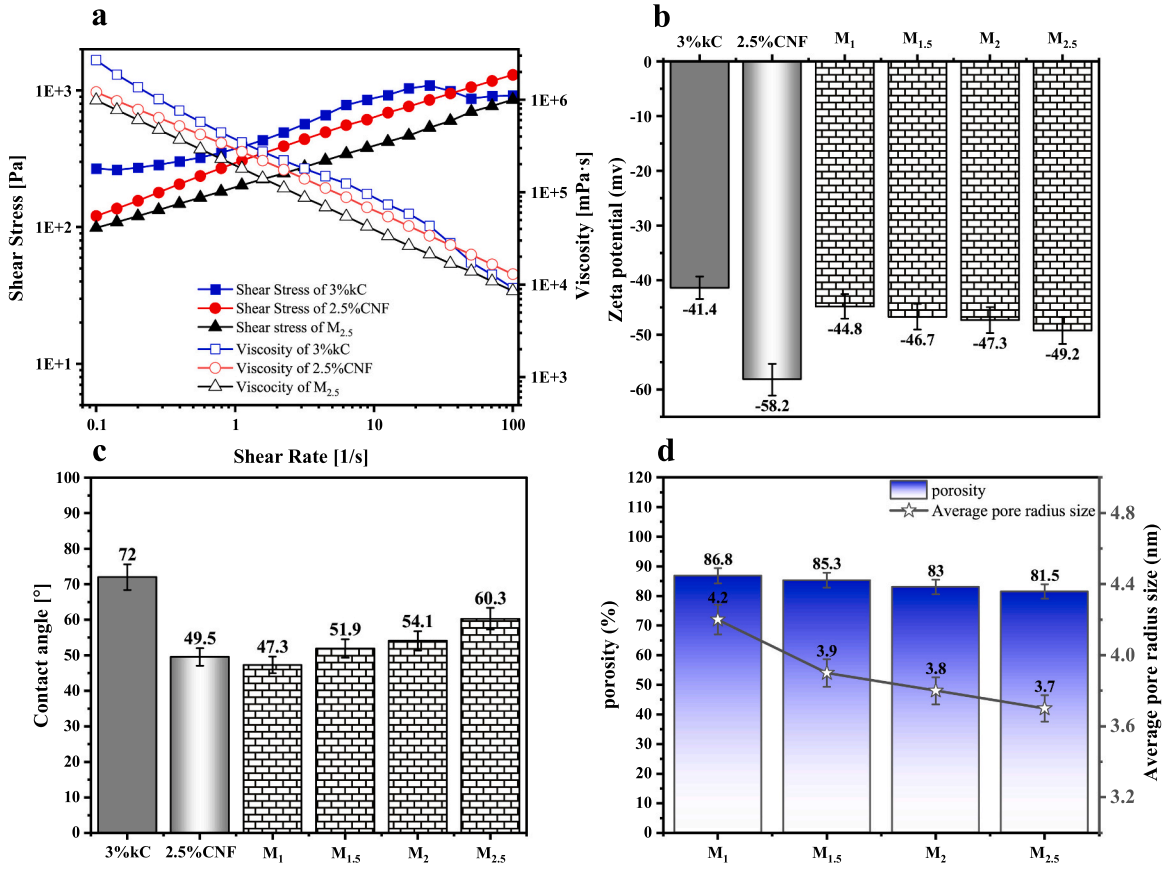

Fig. 2. a) viscosity and shear stress of kC, CNF, and $M_{2.5}$, b) Zeta potential of kC, CNF, M_1, $M_{1.5}$, M_2, and $M_{2.5}$, c) Contact angle measurements of kC, CNF, M_1, $M_{1.5}$, M_2 and $M_{2.5}$, d) porosity and pore size of the composite hydrogel of M_1, $M_{1.5}$, M_2, and $M_{2.5}$.

negative zeta potential (e.g., −40 to −60 mV) prevents aggregation, maintaining the hydrogel structure and increasing surface area for adsorption. The superior increase in negative zeta potential at higher CNF concentrations suggests that such hydrogel formulations could be highly efficient in removing positively charged contaminants from water while keeping structural integrity over time [30], specifically at neutral to basic pH, where the carboxyl groups in CNF are fully deprotonated, and the zeta potential is negative [34]. Notably, a greater hydrogel negative charge also promotes the repulsion of negatively charged pollutants.

The contact angle measurements provide crucial knowledge of hydrogels' wettability and surface features. Fig. 2c shows a contact angle of 72° ± 3.6 for kC, which is the highest contact angle, indicating a relatively low wettability and a more hydrophobic surface. Depending on the concentration of CNF, the kC-CNF hydrogels display various characteristics when crosslinked with GA. The M_1 exhibited the lowest contact angle, 47.3° ± 2.4, indicating the highest possible wettability and the most effective water adhesion. The contact angles steadily rose to 51.9° ± 2.6, 54.1° ± 2.7, and 60.3° ± 3.0 when the concentration of CNF increased to 1.5 %, 2 %, and 2.5 %, respectively, indicating that an increase in CNF leads to a more settled structure and reduces the interaction of water with the surface. These findings highlight that kC-CNF/GO-GA hydrogels are tunable, making them potential candidates for applications that need surface wettability customized to specific applications.

4.2. Porosity and pore size

Enforced with CNF and coated with GO, the GA crosslinked kC membrane has significant potential for desalinating seawater due to its selective absorption capabilities, porosity, and mechanical stability. Fig. 2d shows that incorporating different amounts (1–2.5 %) of CNF within the 3 %kC hydrogel matrix affects the porosity and average pore radius. With increasing CNF concentration, porosity lessened from 86.8 % ± 2.6 at 1 %CNF to 81.5 % ± 2.4 at 2.5 %CNF (Eq. 6), while the average pore radius concurrently reduced from 4.17 nm ± 0.08–3.74 nm ± 0.075 (Eq. 7). GA forms covalent connections between kC and CNF chains, strengthening the hydrogel structure, while GA-induced crosslinking lowers pore size and stabilizes the hydrogel network, making it more durable and performable after multiple filtration cycles. Selectivity-intensive applications recommend a greater CNF concentration, circa 2.5 %, to create a compact network for rejecting ions. Instead, a small amount of CNF, circa 2 %, can balance selectivity and water flux, making it suitable for applications that require good flow and large molecule rejection [9,11].

The top coating layer of 0.05 % GO mixed with 2 % GA enhances the hydrogel's selectivity and makes the surface more stable and fouling-resistant. GO's high surface area and functional groups increase heavy metal separation from the solution, while its hydrophilicity supports water permeability. Thus, the GO/GA layer acts as a selective barrier, capturing ions and pollutants, though it slightly reduces water flux due to denser pore structures [31]. It shows the effect of variation in CNF concentration on the pore structure, changing the ability to adsorb and desorb substances. As CNF concentration increased from 1 % to 2.5 %, the adsorption surface area decreased from 68.5 to 39.25 m^2/g, while pore volume decreased from 0.079 to 0.025 cc/g, and pore radius decreased from 3.75 to 2.98 nm. This pattern shows that more CNF concentration makes the structure dense and less porous by its shorter crosslinks or more physical crosslinks, further improving the antifouling property due to the tighter structure of the hydrogel substrate.

The desorption study also shows a similar pattern, with the surface area decreasing from 62.77 to 36.76 m^2/g. With an increase in the CNF concentration, the diameter of the pore gets smaller, decreasing from 3.62 nm in M_1 to 2.82 nm in $M_{2.5}$. These changes reflect a compact and highly crosslinked network at higher CNF levels, restricting pore size but increasing overall matrix density. GA crosslinking and higher CNF amplify this effect by reinforcing bonds within the structure, further restricting pores' size [17,21].

Table S2(Supplementary Materials) illustrates the BET test of 3 %kC hydrogels with different 1–2.5 % CNF amounts. The pore size difference between the calculated value (3.7 nm) and the BET result (2.8 nm, Table S2) arises from the different measurement principles of the two methods. Eq. (7) provides an estimated hydraulic pore size, while BET measures the textural (gas-accessible) pores.

4.3. Hydrogel swelling, deswelling, and water uptake

The swelling properties of hydrogels in DI water are a critical indicator of their hydrophilic nature, network structure, and capacity to retain water. The microstructural characteristics, particularly crosslinking density, determine hydrogel swelling properties. When kC-CNF hydrogels crosslinked with GA were tested with DI water, their swelling degree decreased with increasing CNF concentration (Fig. 3a). The CNF reinforces the hydrogel network, hence reducing water uptake by restricting polymer chain mobility. The observed trend in swelling follows the calculated decrease in average crosslink length, as discussed in the following section. For example, M_1 exhibited the largest swelling (9.8 g/g ± 0.49), whereas $M_{2.5}$ had the lowest (8.0 g/g ± 0.40). Xu et al. [41] found that network contraction decreased the swelling ratio (SR) with denser polymer crosslinking architectures [41]. According to Bai et al. [6], double-network hydrogels dissipate energy and have excellent anti-swelling properties [6]. Chemically crosslinked hydrogels usually have properties that keep them stable and prevent them from swelling, but making them often requires complicated steps and chemicals [39]. Thus, membranes with elevated CNF concentration consistently displayed lower swelling degrees due to denser crosslinking and less hydrophilicity [8,10,14].

Fig. 3b shows the degree of swelling of M_1, $M_{1.5}$, M_2, and $M_{2.5}$ membranes in 0.5–2.5 g/L NaCl concentrations. There is a strong relationship between the concentration of NaCl and the swelling behavior of kC-CNF/GO-GA hydrogel membranes. The degree of swelling increased with the concentrations of sodium chloride because the ionic strength raises the osmotic pressure inside the hydrogel matrix, increasing the amount of water taken in. Also, neutralizing sulfate groups with Na^+ ions reduces electrostatic repulsion between the polymer chains, expanding the network for more water absorption. For $M_{2.5}$, which exhibits a rise in swelling from 5.4 g/g ± 0.2 at 0.5 g/L to 7.8 g/g ± 0.2 at 2.0 g/L. At 2.5 g/L NaCl concentration, the degree of swelling decreases due to the increased osmotic pressure in the opposite direction that draws water out of the hydrogel membrane. In addition, the stronger electrostatic shielding exerted by 2.5 g/L NaCl solution tightens the polymer chains, limiting the hydrogel's water absorption capacity.

The hydrogels' deswelling behavior was analyzed to understand their structural properties and capacity to retain water (Fig. 3c). Standalone kC deswelling dropped from 64.8 % to 0.2 % after 270 min, while the standalone CNF deswelling dropped from 72 % to 1.5 % after 270 min. The deswelling rates for M_1, $M_{1.5}$, M_2, and $M_{2.5}$ at 30 min were 58.1 %, 70.7 %, 76.8 %, and 86.5 %, respectively, and reached circa 0.7 % after 270 min. The membranes' compact polymer networks, strengthened by GA crosslinking, contributed to better water retention by the crosslinked kC-CNF/GO membranes and decreased water loss over time. Increasing the concentration of CNF improved water retention due to the denser and more stable polymer networks. Swelling and deswelling also induce structural changes in hydrogels and can produce various surface patterns. These surface patterns are stable in both dry and swollen states and enhance the potential of hydrogels for multiple applications [24].

Fig. 3d indicates that as the concentration of CNF increases, there is a corresponding decrease in the membrane water uptake percentage. Specifically, M_1 exhibits the highest water uptake at 2019.3 % ± 101, while $M_{2.5}$ shows the lowest at 1197.5 % ± 60. Based on this pattern, greater concentrations of CNF result in a denser polymer network,

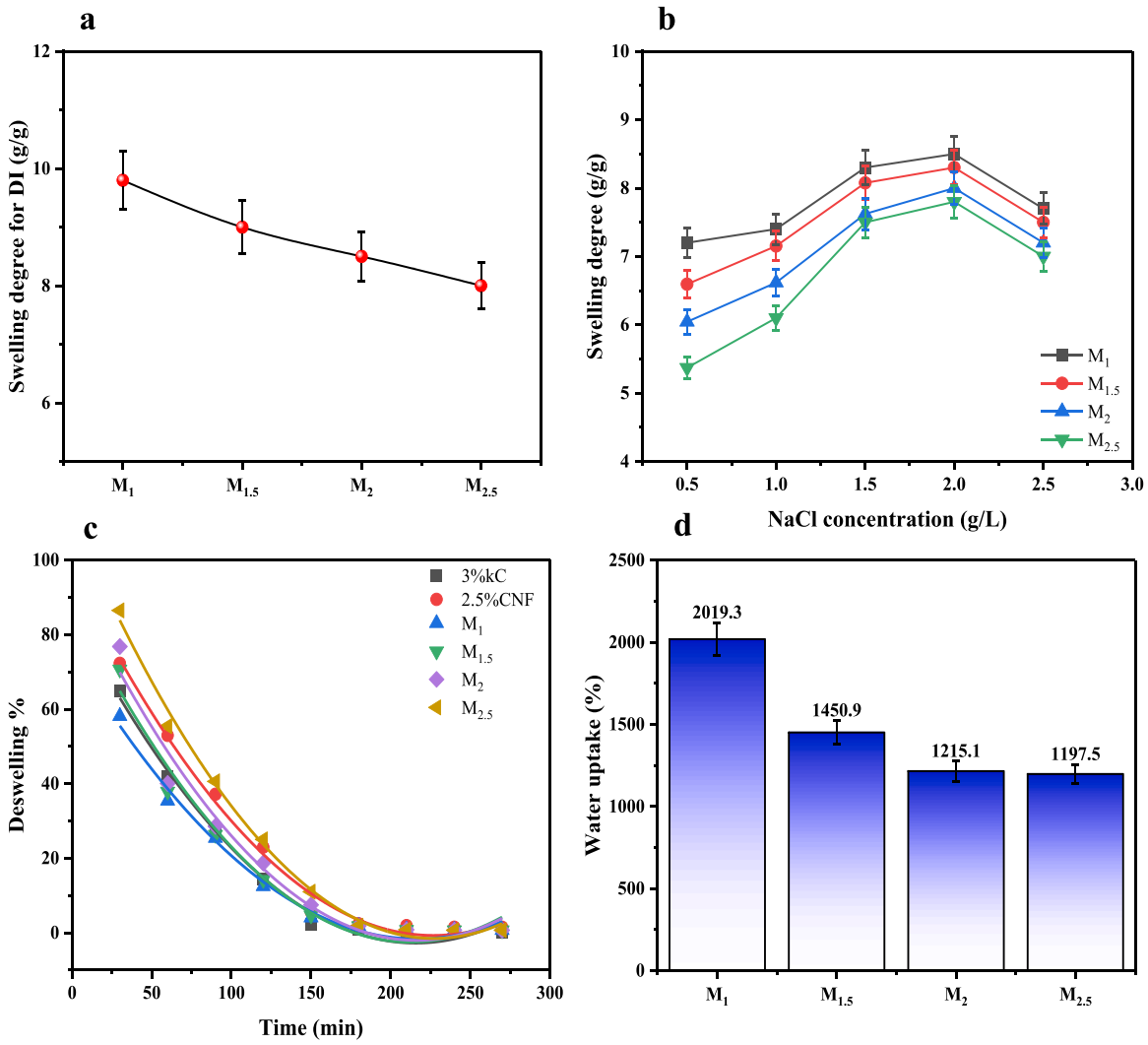

Fig. 3. a) Swelling degree in DI water of M_1, $M_{1.5}$, M_2, and $M_{2.5}$ for 2 h, b) Swelling degree of various hydrogels at various concentrations of NaCl, c) Deswelling of M_1, $M_{1.5}$, M_2, and $M_{2.5}$ hydrogel with time, d)Water uptake ability of M_1, $M_{1.5}$, M_2, and $M_{2.5}$ hydrogel.

reducing the hydrogel's capacity to absorb water. This behavior is consistent with the findings that have been obtained, which state that an increase in the crosslinking density of hydrogels leads to a decrease in the swelling capacity. Therefore, it is feasible to adjust the swelling characteristics of kC-based hydrogels for specific applications by changing the concentrations of CNF.

The hydrogel membranes exhibited swelling and deswelling behaviors controlled by several circumstances. The enhanced crosslinking density results in a denser polymer network, reducing the swelling capacity and limiting the quantity of absorbed water. Although the membrane's mechanical strength increases with the CNF concentration, the water absorption is further restricted owing to the denser network structure. The combined effects of increased crosslinking density and incorporation of CNF resulted in a reduction in porosity and pore size (Fig. 2d), which in turn restricted the amount of space available for water molecules and reduced the swelling capacity.

4.4. Average molecular weight between crosslinks

In this study, the swelling data of the hydrogel samples were used to estimate the M_C values. Due to the complexity of the nanocomposite hydrogel system, particularly the presence of the top GO layer, the Mc calculations were performed based on simplified systems, where the GO layer was excluded. Accordingly, the obtained relative values were used to compare the properties. The calculated M_C was therefore regarded as an effective average molecular weight between all crosslinking points in the hydrogel bulk, integrating both covalent (GA-induced) and physical (CNF/kC) bonds. Full details of the methodology and assumptions used for these approximations, as well as the discussion on the effect of M_C values on hydrogel properties, are provided in the Supplementary Materials.

GA plays a pivotal role as a crosslinker in the hydrogel membrane, forming covalent bonds, mostly with the hydroxyl groups in the CNF and the sulfate and hydroxyl groups in the kC. Such covalent crosslinks establish a stable 3D network, although physical interactions, including hydrogen bonding, ionic bonds, and chain entanglements, also support the stability and performance of the hydrogel. In contrast to covalent bonds, physical interactions are transient and reversible. Nonetheless, they contribute immensely to the hydrogel's mechanical integrity and dimensional stability under operational conditions [13,40,43]. Therefore, the M_C value represents the combined effect of both chemical and physical crosslinking. It reflects the average molecular weight of polymer segments between effective crosslinking points, whether those points are formed via covalent bonds or strong physical associations. As such, variations in Mc can be interpreted as changes in the overall crosslinking density of the hydrogel network, encompassing the full range of interactions that govern its structural and functional behavior [27].

According to the swelling behavior, the estimated Mc values for the M1, M1.5, M2, and M2.5 samples were 10,535.5, 9344.8, 8639.9, and 7914.6 g/mol, respectively. This decreasing trend suggests that increasing CNF content leads to a higher crosslink density within the hydrogel network. The probable mechanism involves improved interactions between the hydroxyl groups in the CNF and the aldehyde groups of GA, which promote the formation of a denser polymer network. As the network becomes more tightly crosslinked, the mesh size is reduced, thereby limiting the available free volume for water absorption. In addition, although CNF is hydrophilic, its network-tightening effect dominates hydrophilicity; thus, MC values are reduced due to lower SD [45].

4.5. Hydrogel membrane characterization

Fig. 4a illustrates FT-IR analysis of M_1, $M_{1.5}$, M_2, and $M_{2.5}$. The analysis indicates that increasing CNF content enhances hydrogen bonding (3200–3400) $cm^{-1}$and C–O incorporation (1000–1100) cm^{-1} while reducing carbonyl C═O intensity 1700 cm^{-1} , indicating improved crosslinking and hydrogel stability. Fig. 4b shows that the FT-IR of the new $M_{2.5}$ hydrogel membrane changes the intensity of its characteristic band when it is exposed to different types of water, such as

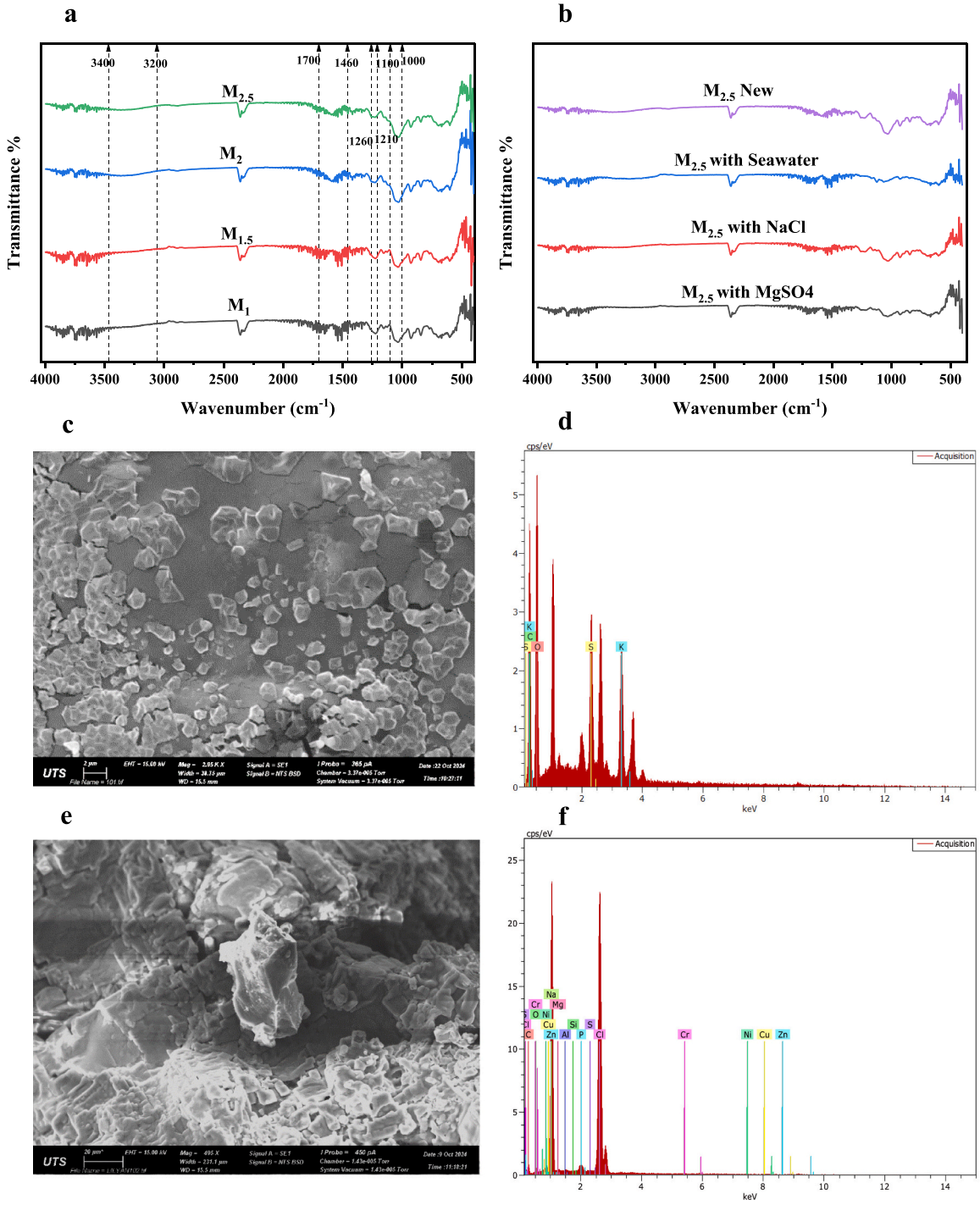

Fig. 4. a) FT-IR of the M_1, $M_{1.5}$, M_2, and $M_{2.5}$, b) FT-IR of the $M_{2.5}$ after filtration with $MgSO_4$, NaCl, and seawater, c and d) SEM and EDS for the new $M_{2.5}$, e, and f) SEM and EDS for the hydrogel after filtration with seawater.

seawater, NaCl, and $MgSO_4$ solutions. Interactions between the hydrogel's functional groups and the ions or molecules in its surroundings affect its swelling behavior, mechanical characteristics, and ion adsorption capacity. For instance, heavy metal ions produce coordination complexes that move the carbonyl stretching area. Saline solutions, such as seawater, NaCl and $MgSO_4$, change the hydrogen bonding network, which can be seen by the stretching of hydroxyl groups in Fig. 4b.

The scanning electron microscopy (SEM) of $M_{2.5}$ hydrogel showed structural alterations. Fig. 4c shows new $M_{2.5}$ has a homogeneous, smooth surface with few fractures and imperfections. The production of crystalline structures, most likely by the deposition of salts and minerals from saline water, caused apparent morphological changes when filtering with seawater (Fig. 4e). The surface of the new hydrogel, which was previously smooth and uniform, has changed due to the deposits on its surface. These deposits provide evidence of metal ions captured by the membrane during seawater filtration.

As shown in Table S3 and Figs. 4d and 4f, the Energy Dispersive X-ray Spectroscopy (EDS) of the $M_{2.5}$ reveals that the composition of the hydrogen goes through changes after the filtration process. Oxygen (49.83 wt%) and carbon (31.03 wt%) are in the new hydrogel structure. Notable levels of sulfur (7.27 wt%) and potassium (11.88 wt%) are also present, indicative of the hydrogel's organic and polysaccharide-based composition. The hydrogel structure changes after seawater filtration.

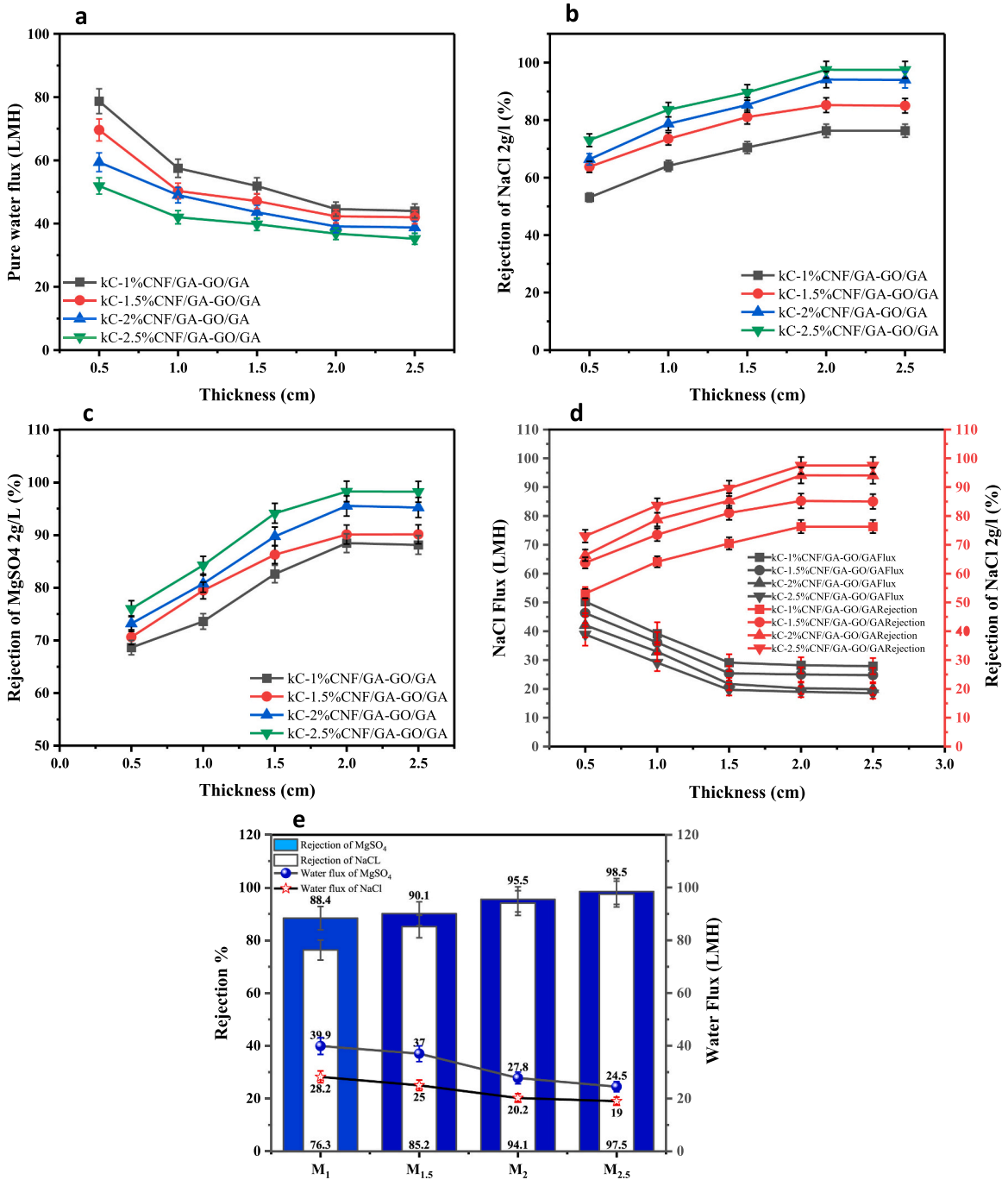

Fig. 5. a) Influence of hydrogel thickness on pure water flux, b) Influence of hydrogel thickness on 2 g/L NaCl rejection, c) Influence of hydrogel thickness on 2 g/L $MgSO_4$ rejection, d) Influence of hydrogel thickness on 2 g/L NaCl rejection and flux, e) Rejection and flux at 2 cm thickness for M_1, $M_{1.5}$, M_2, and $M_{2.5}$ with NaCl, and $MgSO_4$.

Carbon, oxygen, sulfur, and potassium concentrations decreased, suggesting salt replacement of these elements. On the other hand, there is a rise in the concentrations of sodium (31.90 wt%) and chloride (44.23 wt %), indicating a large amount of salt deposition (Fig. 4e).

4.6. Hydrogel DI water flux and salt rejection

DI water feed solution was utilized to evaluate the pure water flux of M_1, $M_{1.5}$, M_2, and $M_{2.5}$ membranes of 0.5, 1, 1.5, 2, and 2.5 cm thicknesses. Notably, hydrogel membrane M_3, with 3 %CNF concentration, was not further considered in the comparison (Fig. 5) due to its low water flux and subtle rejection improvement compared to $M_{2.5}$ (Figures S2a and S2b, Supplementary Materials). Membrane M_3 membrane, with 3 % CNF, is a good example that explains the relationship between CNF concentration and membrane performance, with a slight increase in M3 rejection, 0.4 % to Mg and 0.5 % to Na, due to increased CNF concentration from 2.5 % to 3 % (Figure S2b, Supplementary Materials).

Fig. 5a shows that the water flow declines as the hydrogel membrane's thickness and the CNF concentration increase. The 2 cm thickness membrane stands out with a balanced performance of excellent water flux and solute rejection. Membrane M_1 exhibited the maximum water flux of 78.7 LMH ± 3.9 at 0.5 cm, while the $M_{2.5}$ exhibited the lowest flux of 51.9 LMH ± 2.6 at 0.5 cm. As the thickness of the membrane increased to 2.0 cm, the water flux dropped to 44.6 LMH ± 2.2 for M_1 and 36.8 LMH for $M_{2.5}$, respectively. Increasing the thickness and CNF concentration in hydrogel membranes reduced water flux due to the tighter membrane structure, increased hydrophilicity, and increased hydraulic resistance. Thicker membranes provide increased hydraulic resistance, whereas higher CNF concentration densifies the hydrogel matrix, lowering porosity and permeability. Increasing the CNF content in the hydrogel improves the membrane's structural integrity by forming a more compact network [1]. This densification enhances the membrane's structural stability at the expense of decreased pore size and porosity (Fig. 2d), lowering water permeability.

While GA crosslinking is widely used in the field of hydrogels, its precise influence on hydrogel network structure and filtration properties is not always quantitatively assessed for water purification applications. In this work, M_C calculations offer a molecular-scale understanding of how crosslinking density impacts water permeability and solute rejection. Hence, the observed decrease in DI water flux with increasing CNF content can be further explained by examining the calculated M_C values. MC values decline with increasing CNF concentration, suggesting the formation of a denser and tightly crosslinked hydrogel network. A shorter MC corresponds to shorter polymer chains between crosslinks, which reduces the free volume and limits the number and size of interconnected water channels available for transport. This structural compactness directly prohibits water diffusion through the hydrogel, leading to a noticeable drop in pure water flux. Moreover, although CNF is hydrophilic and could, in theory, enhance water affinity and uptake, the dominating influence of crosslink density appears to override this effect. Water molecules encounter increased resistance due to the denser matrix, which suppresses bulk water transport despite any localized hydrophilicity from cellulose nanofibrils.

Figs. 5b and 5c show an increase in the membranes' rejection with the thickness due to a more effective barrier against salt diffusion. For a 2 g/L NaCl concentration and 0.5 cm thickness, the M_1 exhibited a 53.1 % ± 1.6 rejection rate, increased to 63.8 % ± 1.9 for $M_{1.5}$, reached 66.4 % ± 2.0 for M_2 and 73.0 % ± 2.2 for $M_{2.5}$ membranes. Membranes' rejection increased dramatically at 2 cm, achieving 76.3 % ± 2.3, 85.2 % ± 2.6, 94.1 % ± 2.8, and 97.5 % ± 2.9 for M_1, $M_{1.5}$, M_2, and $M_{2.5}$, respectively. The corresponding membranes' rejection for 2 g/L $MgSO_4$ and 2 cm was 88.4 % ± 1.8 for M_1, 90.1 % ± 1.8 for $M_{1.5}$, 95.5 % ± 1.9 for M_2, and 98.2 % ± 1.9 for $M_{2.5}$ hydrogels. $MgSO_4$, a divalent salt, often exhibits higher rejection than monovalent NaCl due to the size and charge density differences. Fig. 5d indicates that the water flux of NaCl decreased as the thickness and concentration of CNF increased. Specifically, water flux dropped from 50.3 LMH ± 5–27.9 LMH ± 2.8 for the M_1 and from 38.9 LMH ± 3.9–18.5 LMH ± 1.9 for the $M_{2.5}$ membranes. In addition to the physical restrictions imposed by lower M_C values, ionic screening effects from NaCl may reduce osmotic pressure-driven swelling, further reducing water uptake and flux in saline environments. These effects are more evident in samples with higher CNF content and shorter crosslink lengths.

At the same time, the rejection rate improved, increasing from 53.1 % ± 1.6–76.3 % ± 2.2 for the M_1 and 73.01 % ± 2.2–97.5 % ± 2.9 for the $M_{2.5}$. At a thickness of 2 cm, $MgSO_4$ was rejected by the membranes at a higher rate than NaCl. As the CNF concentration increased from 1 % to 2.5 %, the rejection rate for $MgSO_4$ increased from 88.4 % to 98.5 %, whereas NaCl's rejection rate increased from 76.3 % to 97.5 %. On the contrary, water flux for $MgSO_4$ dropped from 39.9 LMH in M_1 to 24.5 LMH in $M_{2.5}$, while for NaCl, it dropped from 28.2 LMH in M_1 to 19 LMH for NaCl $M_{2.5}$, indicating a reduction in the water flux at higher CNF concentrations (Fig. 5e). For both $MgSO_4$ and NaCl feeds, the reduction in water flux at higher CNF concentrations was due to a decrease in the membrane's pore size that enhances its selectivity but reduces the water permeability. However, the greater rejection of $MgSO_4$ can be attributed to the larger hydrated radius of the Mg^{2+} ion (0.428 nm) compared to that of the Na^+ ion (0.276 nm), as well as the divalent valency of Mg^{2+} that encounters greater attraction by the negatively charged membrane surface. In contrast, the monovalent Na^+ ions are able to pass through more quickly.

In all membranes, kC offers the fundamental structure with sulfate groups that engage with water and ions. At the same time, GA functions as a crosslinking agent to enhance the hydrogel's strength and reduce pore size, while the graphene oxide top layer increases the surface area and introduces functional groups that enhance the membrane's adsorption and mechanical stiffness. The concentration of CNF is critical to forming a denser hydrogel network of reduced pore sizes and augmented zeta potential for better ion rejection. A denser hydrogel matrix enhances the membrane's selectivity, improving the rejection of ions, and smaller pore sizes restrict ion passage, increasing ions' rejection [16].

The Mc values influence the hydrogel membranes' rejection of NaCl and $MgSO_4$ salts. Mc values decreased with increasing concentration of CNF, reflecting shorter distances between crosslinking points and a denser three-dimensional network. This tighter structure played a critical role in modulating ion transport and improving salt rejection efficiency. For both salts, lower Mc values enhanced the membrane's ability to act as a size-exclusion barrier. A smaller free volume within the matrix restricts the diffusion of solvated ions, especially those with large hydration shells, such as Mg^{2+} and SO_4^{2-}. This effect contributed to the consistently higher rejection rates observed for $MgSO_4$ compared to NaCl, as the hydrated Mg^{2+} ion (~8.6 Å) is substantially larger than Na^+ (~7.2 Å). The denser networks effectively limited the passage of these larger species while partially allowing smaller or monovalent ions to permeate.

In addition, the reduced Mc enhances the Donnan exclusion mechanism by maintaining a more compact hydrogel structure. This can concentrate fixed charges in the network (e.g., carboxyl or hydroxyl groups from CNF or gelatin), which repel co-ions and reinforce the selectivity against multivalent ions. Although CNF is not strongly charged, the overall architecture and spatial constraint provided by a tighter network amplify these electrostatic exclusion effects. Therefore, it can be concluded that while lower Mc values decrease water flux, they improve salt rejection—especially for multivalent salts—by narrowing transport pathways and enhancing charge-based selectivity. The results highlight a fundamental trade-off in membrane design, where tighter networks (lower Mc) enhance selectivity, they also reduce permeability, and an optimal balance must be tailored to application needs.

Thus, permselectivity of the hydrogel membranes is a trade-off between their rejection and water flux, with the membranes' water flux

decreasing as their rejection increases. Since membrane $M_{2.5}$ at 2 cm thickness exhibited the best permselectivity, it was used for seawater desalination in multiple filtration cycles to evaluate its performance over time.

4.7. Seawater desalination

$M_{2.5}$ membrane was tested for seawater desalination experiments in a dead-end filtration column to achieve a recovery rate of 90 %. In the two-stage filtration process, the permeate from the first stage was the feed for the second filtration stage, using a new hydrogel in each stage. In the first stage, the seawater TDS reduced from 34788 mg/L to 3500 mg/L, while it further reduced to 692 mg/L in the second stage. About a 98 % reduction in ion concentration was achieved after the second filtration stage, as shown in Fig. 6a, with the concentrations of Na^+ and SO_4^{2-} in the second stage permeate being 199 mg/L and 21 mg/

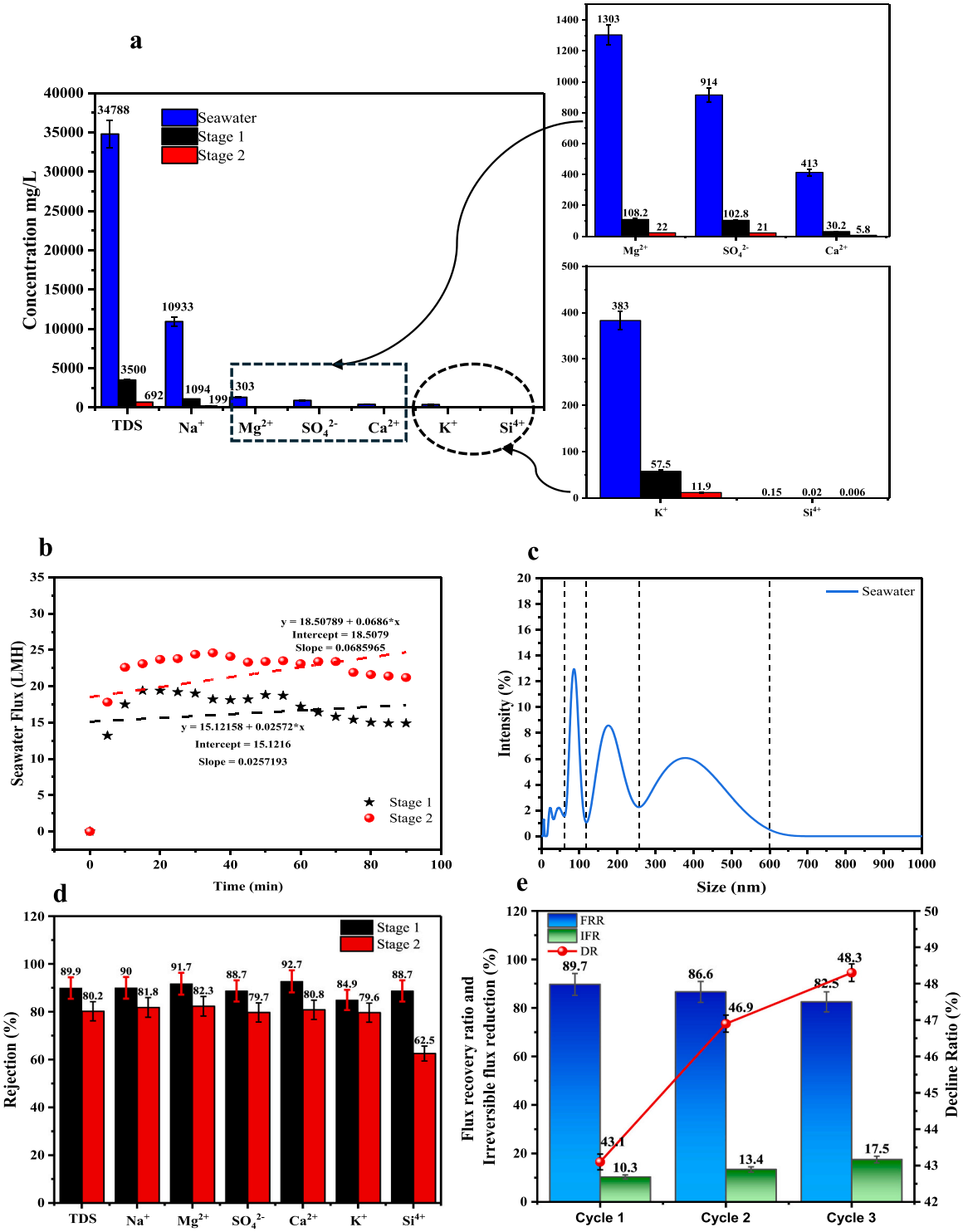

Fig. 6. a) Ion rejection and TDS reduction performance of $M_{2.5}$ hydrogel by seawater, stage 1, and stage 2, b) Water flux of the seawater with time for stage 1, and 2, c) Particle size distribution of the seawater conducted through the Malvern Particle Analyser, d) Removal of contaminants from seawater using $M_{2.5}$ for stage 1, and 2, e) Fouling (FRR, DR, and IFR) % for $M_{2.5}$ with seawater for three cycles.

L. The water flux in the first and second stages is shown in Fig. 6b. In the first filtration stage, a stable water flux of 19.4 LMH was recorded after 20 min and dropped to 14.9 LMH after 90 min, whereas water flux in the second stage was 24.6 LMH after 35 min and decreased to 21.2 LMH after 90 min.

The drop in the water flux in stages one and two can be attributed to scale fouling from divalent ions deposition on the membrane surface, causing pore blockage. The EDX analysis shows divalent ion peaks on the $M_{2.5}$ membrane surface, including Mg^{2+} 0.12 wt%, Si^{4+} 0.02 wt%, and Cu^{2+} 0.24 wt% (Table S3, supplementary material. Compared to divalent ions, Na^{+} and K^{+} exhibit low fouling characteristics due to weaker interaction with the membrane and their high solubility in solution, while Mg^{2+} and Ca^{2+} form complexes with negatively charged molecules, such as sulfate and carbonate, leading to the precipitation of insoluble salts. A gradual decline in water flux, therefore, was inevitable over time, particularly when the membrane operates at 90 %. The dead-end filtration of seawater also promotes fouling due to the accumulation of fouling materials on the membrane surface. The seawater was analyzed through a Malvern Particle analyzer for particle size distribution to study colloidal fouling (Fig. 6c). Results show three peaks of particle size, 250–650 nm, 120–250 nm, and 60–120 nm, which are responsible for membrane fouling by blocking the 2.82 nm pore radius of the $M_{2.5}$ membrane (Table S2, Supplementary Materials).

The first filtration stage exhibited higher overall rejection percentages than the second stage, i.e., 89.9 % vs. 80.2 % (Fig. 6d). For divalent ions, the membrane rejection of Mg^{2+} and Ca^{2+} was 91.7 % ± 4.6 and 92.7 % ± 4.6 in the first stage and 82.3 % ± 4.1 and 80.4 % ± 4.0 in the second stage. The greater Mg^{2+} and Ca^{2+} rejection in stage one was due to the high charge densities of ions that strengthened electrostatic repulsion with the negatively charged functional groups, such as carboxylate ($-COO^{-}$) and sulfate ($-SO_3^{-}$), of the membrane. Compared to Mg^{2+} and Ca^{2+}, SO_4^{2-} was rejected at a lower rate, 88.7 % ± 4.4 in stage one and 79.7 ± 3.9 in stage two, due to its large size and lower charge density, which is responsible for its faster diffusion rate. Also, SO_4^{2-} can shed its large hydration shell more easily than Mg^{2+} and Ca^{2+}. Negatively charged membranes repel anions and attract cations through electrostatic interactions. Despite the more negative zeta potential at 2.5 % CNF loading, the rejection of SO_4^{2-} was lower than that of Mg, which results from ion interactions with the membrane structure. The hydrated radius of SO_4^{2-} is significantly larger than that of Mg^{2+}, resulting in weaker electrostatic exclusion due to steric hindrance within the membrane pores. Moreover, SO_4^{2-} possesses a lower charge density and a more flexible hydration shell, allowing partial dehydration and diffusion through nanochannels. In contrast, Mg^{2+}, with a higher charge density, forms stronger electrostatic interactions with negatively charged groups such as $–COO^{-}$ and $–SO_3^{-}$, enhancing its rejection. The heterogeneous surface charge distribution of the kC–CNF/GA-GO-GA hydrogel may also create localized pathways of lower repulsion potential, further contributing to the relatively lower SO_4^{2-} rejection [26,32]. For Na^{+}, the rejection was 90 % ± 4.5 in stage one and 81.8 % ± 4.0 in stage two, while K^{+} rejection was 84.9 % ± 4.2 in stage one and 79.6 % ± 3.9 in stage two. The lower rejection rate of K^{+} is owing to its greater ionic radius (0.132 nm) and lower charge density, which attenuates the influences of steric and electrostatic exclusion mechanisms. Compared to NaCl binary feed solution experiments, the lower Na^{+} rejection in the seawater experiment is attributed to the complex ionic composition, competitive transport effects in natural seawater, which influence electrostatic exclusion and diffusion mechanisms. Also, the concentration of the feed solution in the NaCl experiment is 2 g/L, while in the seawater experiment is 34788 mg/L, which increases salt leakage across the hydrogel membrane.

Fig. 6e shows the $M_{2.5}$ membrane's performance in three seawater filtration cycles. The same membrane was used in the filtration cycles, with 1-hour DI water cleaning between cycles. The $M_{2.5}$ membrane exhibited an FRR% of 89.7 % ± 4.5 in cycle 1, 86.6 % ± 4.3 in cycle 2, and 82.3 % ± 4.1 in cycle 3, maintaining above 80 % water flux recovery and strong capability for reuse in multiple filtration cycles. The IFR% was 10.3 % ± 0.8 in the first cycle and increased to 17.5 % ± 1.4 by the third cycle, indicating a gradual buildup of irreversible fouling due to the inadequate removal of pollutants by the DI water cleaning. However, the IFR increase was moderate, implying the durability and ability of the membrane to maintain functionality despite repeated use at a 90 % recovery rate. The DR% increased from 43.1 % ± 0.21 in cycle 1–48.3 % ± 0.24 in cycle 3 as a result of membrane fouling. Seawater changes the hydrogen bonding network in the $M_{2.5}$ membrane, which can be seen by the stretching of hydroxyl groups in Fig. 4b and a rise in the concentrations of sodium (31.66 wt%), chloride (44.23 wt%), and silica (0.02 wt%), indicating a large amount of salt deposition (Table S3, supplementary material). Membrane fouling was inevitable due to the elevated recovery rate in the filtration cycles and inadequate cleaning. The SEM images of the new and used hydrogel show an accumulation of fouling materials on the membrane surface after the seawater filtration (Figs. 4c and 4e). The EDS images (Figs. 4d and 4f) confirm high peaks of sulfate, silica, and divalent ions on the surface of the fouled membrane after seawater filtration (Fig. 4f), indicating silica and metal sulfate fouling, such as magnesium sulfate. Fig. 4b shows FT-IR spectra of the M2.5 hydrogel before and after exposure to NaCl, $MgSO_4$, and seawater, revealing spectral shifts in the O–H (3140–3380 cm^{-1}), C═O (1650–1700 cm^{-1}), S═O (1215–1240 cm^{-1}), and C–O–C (1030–1060 cm^{-1}) regions. These changes indicate ion–polymer interactions and hydrogen-bond rearrangement. The fouling propensity of the hydrogel membrane was severely exacerbated by the elevated recovery rate of the filtration process and membrane cleaning with DI water only, which is ineffective in the removal of silica and metal sulfate precipitates.

Table S6 (supplementary material) summarizes a comparison of research on CNF, GO, and kC hybrid membranes for water purification. The table shows water flux, rejection, and water flux recovery ratio (FRR) for several studies. In general, the water flux, FRR, and rejection rate of the kC-CNF/GO-GA are similar or competitive to those reported in the literature. Notably, the hydrogel membrane in this study is gravity-driven and hence does not require high energy for seawater desalination. Additionally, the hydrogel membrane operates at a 90 % recovery rate, which is challenging for most pressure-driven membrane processes. Previous studies [4,28] fabricated a GO-based membrane for dye removal from wastewater. Although the studies reported 90–95 % rejection of dyes, the rejection of divalent and monovalent ions was between 75 % and 80 %. Subsequent studies optimized the crosslinking and the composite design to enhance mechanical stability, ion selectivity, and antifouling performance of the GO NF membrane [22]. Nevertheless, the membrane exhibited 95 % removal of dyes and water flux recovery of 85 % while water flux recovery in this study was 89.7 % at a 90 % recovery rate. In later studies, Kardani et al. fabricated a GO/PEI and hole-enriched GO/CNF membrane [19], with superior ion transport and mechanical reinforcement for heavy metal recovery from wastewater. The membrane, with 93 % rejection on NaCl and 94–99 % rejection of divalent ions, exhibited a low water flux of 7.72 LMH and 90.93 % FRR. The current kC–CNF/GO–GA hydrogel integrates a sustainable biopolymer with excellent ion rejection (≈98 %) and water flux, providing a cost-effective solution for seawater desalination. The gravity-driven membrane achieved a 90 % recovery rate and 89.7 % FRR after three cycles of seawater filtration and DI water cleaning.

4.8. Reusability

Desorption and reuse of the $M_{2.5}$ membrane are very important in practical applications from an economic point of view. Fig. 7a illustrates the highest relative desorption capacity of $MgSO_4$ and NaCl in a 2 g/L solution. Consecutive adsorption/desorption cycles were performed to assess the membrane reusability. The results show the robust adsorption/desorption characteristics of the $M_{2.5}$ membrane, even after three filtration cycles, with an adsorption efficiency of 79.4 % ± 3.2 for Na^{+}

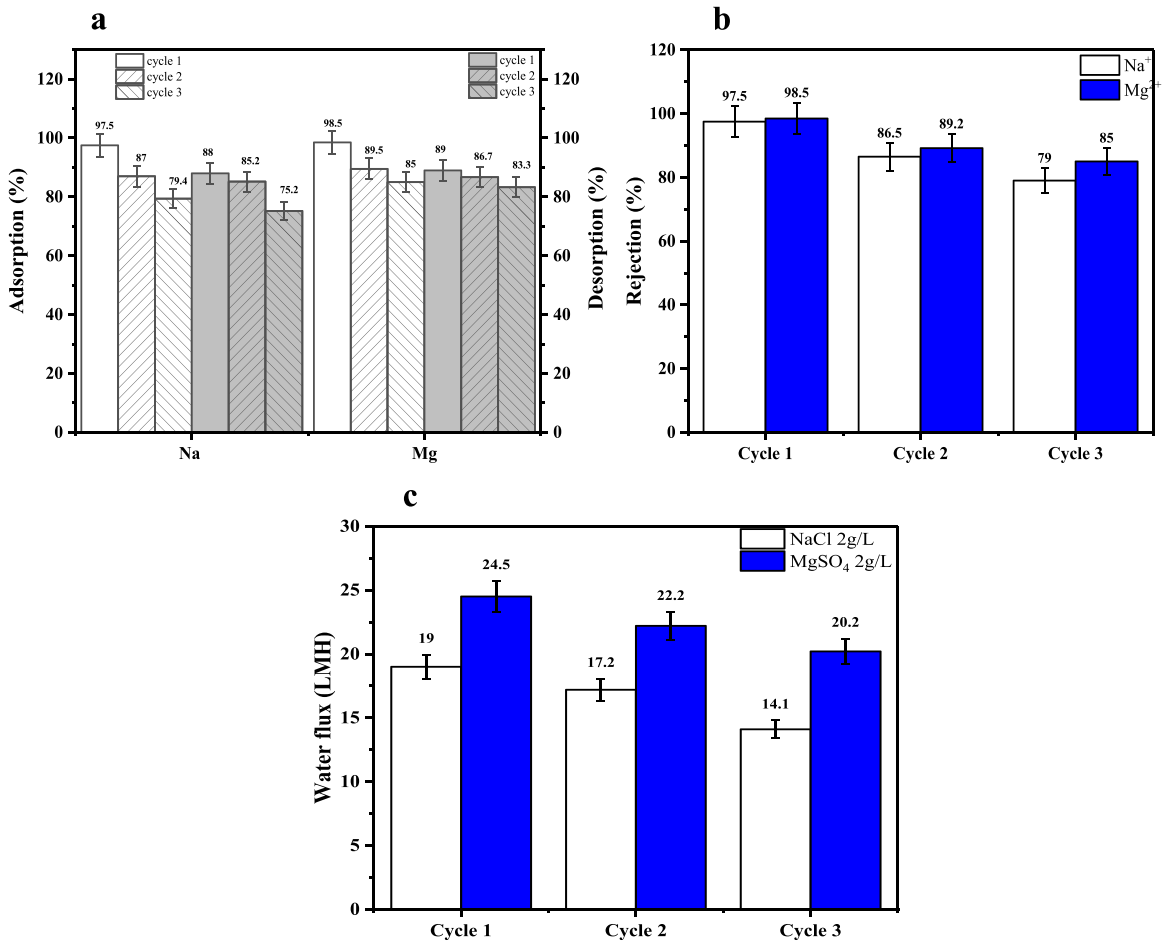

Fig. 7. a) Adsorption/desorption cycles for 2 g/L NaCl and $MgSO_4$ on the $M_{2.5}$, b) Rejection of 2 g/L NaCl and $MgSO_4$ during three cycles by $M_{2.5}$, and c) Water flux of NaCl 2 g/L and $MgSO_4$ 2 g/L during three cycles by $M_{2.5}$.

and 85 % ± 3.4 for Mg^{2+} and a desorption efficiency of 75.2 % ± 3 for Na^+ and 83.3 % ± 3.3 for Mg^{2+}.

The efficiency of the $M_{2.5}$ membrane was also evaluated in multiple filtration cycles to investigate the rejection and water flux. After three filtration cycles, a reasonable reduction was noted in the rejection of $MgSO_4$ from 98.5 % ± 4.9–85 % ± 4.3 and for NaCl from 97.5 % ± 4.9–79 % ± 3.9. Water flux also dropped from 24.5 LMH ± 1.2 in cycle one to 20.2 LMH ± 1.0 in cycle three in the $MgSO_4$ tests and from 19 LMH ± 0.95 in cycle one to 14.1 LMH ± 0.71 in cycle three in the NaCl tests. The decline in the water flux was a consequence of Mg^{2+} and Na^+ ions blocking the hydrogel's porous network. The $M_{2.5}$ membrane was rinsed with DI water between filtration cycles to remove the easily attached fouling materials. However, deeper impurities remain within the membrane structure, reducing water flux (Figs. 7b and 7c). Consequently, the $M_{2.5}$ hydrogel membrane can be an efficient adsorbent to remove divalent and monovalent ions in multiple filtration cycles since it can rapidly and effectively regenerate. The GO–GA layer exhibited strong adhesion to the hydrogel surface under dead-end filtration conditions, maintaining stability over three filtration cycles under 0.5 bar pressure. Minor delamination was observed after extending the filtration cycling due to normal interfacial fatigue during repeated swelling–deswelling, rather than poor adhesion of the GO-GA layer. Given that the membranes were designed for batch ion-removal and recovery applications rather than long-term continuous operation, the observed stability was satisfactory for their intended use. Nevertheless, future studies can focus on the improvement of interfacial bonding strategies to enhance long-term durability.

Based on retail prices, the cost of the filtration system, including the hydrogel filter for multiple uses, is very reasonable. The hydrogel costs about AU$6 per m^3 (of 2 cm thickness), producing more than 15 LMH of desalinated water from seawater. The kC-CNF/GA-GO/GA hydrogel filter has a long shelf life, as long as it is kept in a closed container, and it would remain effective at least for more than a year from the date of preparation.

5. Conclusion

A gravity-driven kC-CNF composite hydrogel coated with GO and crosslinked with GA was fabricated for seawater desalination in stages from 34788 mg/L to 692 mg/L. The permeate water TDS falls within the fair water quality, TDS between 600 and 900 mg/L, which is applicable for irrigation and general use. Further treatment to reduce the TDS to ≤ 500 mg/L is required for drinking use. The water flux reduces when the concentration of CNF increases in the hydrogel from 1 % to 2.5 %; in contrast, the rejection increases. CNF addition increased membrane stiffness and altered its structure, as evidenced by different analyses. The membranes were tested with DI water, NaCl and $MgSO_4$ solutions, and real seawater. Increasing CNF content lowered water and salt solution fluxes while enhancing NaCl and $MgSO_4$ rejection. This behavior was linked to the calculated M_C values, which decreased with CNF content, indicating a denser and more tightly crosslinked network. Such networks limited water mobility but improved selectivity and salt rejection.

The best hydrogel was the $M_{2.5}$ hydrogel, which achieved a rejection rate of 98.5 % ±5 for divalent ions and 97.5 % ±5 for monovalent ions. Furthermore, the hydrogel demonstrated a significant water flow, ranging from 24.5 LMH to 19 LMH for synthetic feed solutions and 18

LMH for seawater. The hydrogel exhibits efficient and selective ion extraction from saline solutions, with high rejection rates of 90 % for Na^+, 91.7 % for Mg^{2+}, and K^+ has a lower rejection rate of 84.9 %. The hydrogel showed robustness to fouling conditions with a flux recovery ratio of 89.7 % ± 4.5 for seawater 35 g/L with a decline ratio (DR) of 43.1 ± 0.2 %. The hydrogel membrane exhibited 82.5 % FRR after three filtration cycles with seawater. These results show the potential of molecular-level tailoring of hydrogels in allowing precise control over hydrogel behavior and performance. The next steps should be scaled manufacturing, real-world antifouling testing, and hydrogel regenerating capabilities. While this study focused on the optimization of the CNF crosslinking, the GA crosslinking degree and GO coating thickness should be further investigated in further studies to optimize the rejection-flux trade-off. The kC-2.5 %CNF/GO-GA hydrogel is a major step towards sustainable and creative environmental solutions.

CRediT authorship contribution statement

Yahia Aedan: Validation, Investigation. **Abdulmajeed Al Askar:** Methodology, Formal analysis, Data curation. **Alaa H. Hawari:** Validation, Funding acquisition, Formal analysis, Data curation. **Faris Hamdi:** Writing – review & editing, Methodology, Investigation, Formal analysis. **Hossein Ali Khonakdar:** Writing – review & editing, Visualization, Validation, Formal analysis, Data curation. **Ejji Maryam AL:** Validation, Funding acquisition, Formal analysis, Data curation, Conceptualization. **Ali Altaee:** Writing – review & editing, Writing – original draft, Validation, Supervision, Resources, Investigation, Funding acquisition, Formal analysis, Data curation. **Armaghan Moghaddam:** Writing – review & editing, Writing – original draft, Validation, Investigation, Formal analysis, Data curation. **Lilyan Alsaka:** Writing – review & editing, Writing – original draft, Validation, Investigation, Formal analysis, Data curation, Conceptualization.

Declaration of Competing Interest

The authors declare that they have no known competing financial interests or personal relationships that could have appeared to influence the work reported in this paper.

Acknowledgement

This research is made possible by a food security research award (MME03–1015–210003) from the Qatar National Research Fund (QNRF) in partnership with the Ministry of Municipality. The statements made herein are solely the responsibility of the authors.

Appendix A. Supporting information

Supplementary data associated with this article can be found in the online version at doi:10.1016/j.jece.2025.120445.

Data availability

Data will be made available on request.

References

[1] S. Acarer-Arat, İ. Pir, M. Tufekci, S. Güneş-Durak, A. Akman, N. e Tufekci, Heavy metal rejection performance and mechanical performance of cellulose-nanofibril-reinforced cellulose acetate membranes, ACS Omega 9 (41) (2024) 42159–42171.
[2] S. Ahmed, A. Soundararajan, Marine polysaccharides: Advances and multifaceted applications, CRC Press, 2018.
[3] K. Ali, M. Wahba, R. Abou-Zeid, S. Kamel, Development of carrageenan modified with nanocellulose-based materials in removing of Cu 2+, Pb 2+, Ca 2+, Mg 2+, and Fe 2+, Int. J. Environ. Sci. Technol. 16 (2019) 5569–5576.
[4] C. Ao, W. Yuan, J. Zhao, X. He, X. Zhang, Q. Li, T. Xia, W. Zhang, C. Lu, Superhydrophilic graphene oxide@ electrospun cellulose nanofiber hybrid membrane for high-efficiency oil/water separation, Carbohydr. Polym. 175 (2017) 216–222.
[5] N.B. Baghbadorani, T. Behzad, N. Etesami, P. Heidarian, Removal of Cu2+ ions by cellulose nanofibers-assisted starch-g-poly (acrylic acid) superadsorbent hydrogels, Composites Part B Engineering 176 (2019) 107084.
[6] C. Bai, Q. Huang, X. Zhang, X. Xiong, Mechanical strengths of hydrogels of poly (N, N-Dimethylacrylamide)/Alginate with IPN and of Poly (N, N-Dimethylacrylamide)/Chitosan with Semi-IPN microstructures, Macromol. Mater. Eng. 304 (11) (2019) 1900309.
[7] F.T.P. Borges, G. Papavasiliou, F. Teymour, Characterizing the molecular architecture of hydrogels and crosslinked polymer networks beyond Flory–Rehner—I. Theory, Biomacromolecules 21 (12) (2020) 5104–5118.
[8] C. Chang, M. He, J. Zhou, L. Zhang, Swelling behaviors of pH-and salt-responsive cellulose-based hydrogels, Macromolecules 44 (6) (2011) 1642–1648.
[9] Y. Chen, L. Zhang, Y. Yang, B. Pang, W. Xu, G. Duan, S. Jiang, K. Zhang, Recent progress on nanocellulose aerogels: preparation, modification, composite fabrication, applications, Adv. Mater. 33 (11) (2021) 2005569.
[10] S. Distantina, F. Fadilah, M. Kaavessina, Swelling behaviour of kappa carrageenan hydrogel in neutral salt solution, Int. J. Chem. Mol. Eng. 10 (8) (2016) 998–1001.
[11] S. Distantina, R. Rochmadi, M. Fahrurrozi, W. Wiratni, Preparation and characterization of glutaraldehyde-crosslinked kappa carrageenan hydrogel, Eng. J. 17 (3) (2013) 57–66.
[12] P.J. Flory, J. Rehner Jr, Statistical mechanics of cross-linked polymer networks II. Swelling, J. Chem. Phys. 11 (11) (1943) 521–526.
[13] S. Grabska-Zielińska, Cross-linking agents in three-component materials dedicated to biomedical applications: a review, Polymers 16 (18) (2024) 2679.
[14] H. Hezaveh, I.I. Muhamad, Effect of natural cross-linker on swelling and structural stability of kappa-carrageenan/hydroxyethyl cellulose pH-sensitive hydrogels, Korean J. Chem. Eng. 29 (2012) 1647–1655.
[15] Y. Huang, S. Zou, Z. Li, B. Na, S. Lin, S. Zhang, Tough polyamidoxime-nanocellulose supramolecular composite hydrogels for effective uranium extraction from seawater, Polymer 298 (2024) 126895.
[16] I. Ibrar, L. Alsaka, S. Yadav, A. Altaee, J.L. Zhou, H.K. Shon, Kappa carrageenan-vanillin composite hydrogel for landfill leachate wastewater treatment, Desalination 565 (2023) 116826.
[17] K. Kalaiselvi, S. Mohandoss, N. Ahmad, M.R. Khan, R.K. Manoharan, Adsorption of Pb2+ ions from aqueous solution onto porous kappa-carrageenan/cellulose hydrogels: isotherm and kinetics study, Sustainability 15 (12) (2023) 9534.
[18] E. Karbassiyazdi, A. Altaee, I. Ibrar, A. Razmjou, L. Alsaka, N. Ganbat, A. Malekizadeh, R. Ghobadi, H. Khabbaz, Fabrication of carbon-based hydrogel membrane for landfill leachate wastewater treatment, Desalination (2023) 116783.
[19] R. Kardani, A. Altaee, A. Moghaddam, H.A. Khonakdar, A.K. Samal, J. Zhou, Y. Choo, Nanocomposite kappa-carrageenan-GO/PEI membrane for wastewater valorization and metals recovery, Chem. Eng. J. (2025) 168932.
[20] C.H. Kim, H.J. Youn, H.L. Lee, Preparation of surface-charged CNF aerogels and investigation of their ion adsorption properties, Cellulose 24 (2017) 2895–2902.
[21] V. Kokol, V. Vivod, Cation-exchange performance of a citric-acid esterified cellulose nanofibrous membrane for highly-selective proteins' permeability and adsorption capacity, Carbohydr. Polym. 318 (2023) 121134.
[22] P. Kong, Z. Sun, H. Gui, Z. Chen, Y. Song, Y. Wang, Y. Wang, M.J. Kipper, J. Tang, L. Huang, Advances in the application of graphene oxide composite loose nanofiltration membranes for dye and salt separation, J. Environ. Chem. Eng. 12 (6) (2024) 114278.
[23] P. Kulal, V. Badalamoole, Hybrid nanocomposite of kappa-carrageenan and magnetite as adsorbent material for water purification, Int. J. Biol. Macromol. 165 (Pt A) (2020) 542–553, https://doi.org/10.1016/j.ijbiomac.2020.09.202.
[24] N. Kumar, R. Gusain, S. Pandey, S.S. Ray, Hydrogel nanocomposite adsorbents and photocatalysts for sustainable water purification, Adv. Mater. Interfaces 10 (2) (2023) 2201375.
[25] D. Li, K. Londhe, K. Chi, C.S. Lee, A.K. Venkatesan, B.S. Hsiao, Functionalized bio-adsorbents for removal of perfluoroalkyl substances: a perspective, AWWA Water Sci. 3 (6) (2021) e1258.
[26] L. Liu, S. Lin, X. Xu, Y. Wan, W. Song, J. Luo, Preference of negatively charged membranes in magnesium and lithium separation by nanofiltration, Nat. Commun. 16 (1) (2025) 5731.
[27] L. Lu, S. Yuan, J. Wang, Y. Shen, S. Deng, L. Xie, Q. Yang, The formation mechanism of hydrogels, Curr. Stem Cell Res. Ther. 13 (7) (2018) 490–496.
[28] Y. Lyu, Q. Zhang, Z. Wang, J. Pu, A graphene oxide nanofiltration membrane intercalated with cellulose nano-crystals, BioResources 13 (4) (2018) 9116–9131.
[29] N. Mahfoudhi, S. Boufi, Nanocellulose as a novel nanostructured adsorbent for environmental remediation: a review, Cellulose 24 (2017) 1171–1197.
[30] N. Mohammed, N. Grishkewich, K.C. Tam, Cellulose nanomaterials: promising sustainable nanomaterials for application in water/wastewater treatment processes, Environ. Sci. Nano 5 (3) (2018) 623–658.
[31] S. Mohammed, H.M. Hegab, R. Ou, Nanofiltration performance of glutaraldehyde crosslinked graphene oxide-cellulose nanofiber membrane, Chem. Eng. Res. Des. 183 (2022) 1–12.
[32] D. Pintossi, C.-L. Chen, M. Saakes, K. Nijmeijer, Z. Borneman, Influence of sulfate on anion exchange membranes in reverse electrodialysis, npj Clean. Water 3 (1) (2020) 29.
[33] M.C. Rocha de Souza, C.T. Marques, C.M. Guerra Dore, F.R. Ferreira da Silva, H. A. Oliveira Rocha, E.L. Leite, Antioxidant activities of sulfated polysaccharides from brown and red seaweeds, J. Appl. Phycol. 19 (2007) 153–160.
[34] H. Shaghaleh, Y.A. Hamoud, X. Xu, S. Wang, H. Liu, A pH-responsive/sustained release nitrogen fertilizer hydrogel based on aminated cellulose nanofiber/cationic

copolymer for application in irrigated neutral soils, J. Clean. Prod. 368 (2022) 133098.
[35] J. Štefelová, V. Slovák, G. Siqueira, R.T. Olsson, P. Tingaut, T. Zimmermann, H. Sehaqui, Drying and pyrolysis of cellulose nanofibers from wood, bacteria, and algae for char application in oil absorption and dye adsorption, ACS Sustain. Chem. Eng. 5 (3) (2017) 2679–2692.
[36] C. Tian, J. She, Y. Wu, S. Luo, Q. Wu, Y. Qing, Reusable and cross-linked cellulose nanofibrils aerogel for the removal of heavy metal ions, Polym. Compos. 39 (12) (2018) 4442–4451.
[37] A. Tshikovhi, S.B. Mishra, A.K. Mishra, Nanocellulose-based composites for the removal of contaminants from wastewater, Int. J. Biol. Macromol. 152 (2020) 616–632.
[38] S. Wang, X. Ma, P. Zheng, Sulfo-functional 3D porous cellulose/graphene oxide composites for highly efficient removal of methylene blue and tetracycline from water, Int. J. Biol. Macromol. 140 (2019) 119–128.
[39] X. Xiang, G. Chen, K. Chen, X. Jiang, L. Hou, Facile preparation and characterization of super tough chitosan/poly (vinyl alcohol) hydrogel with low temperature resistance and anti-swelling property, Int. J. Biol. Macromol. 142 (2020) 574–582.
[40] J. Xu, M. Zhang, W. Du, J. Zhao, G. Ling, P. Zhang, Chitosan-based high-strength supramolecular hydrogels for 3D bioprinting, Int. J. Biol. Macromol. 219 (2022) 545–557.
[41] S. Xu, H. Li, H. Ding, Z. Fan, P. Pi, J. Cheng, X. Wen, Allylated chitosan-poly (N-isopropylacrylamide) hydrogel based on a functionalized double network for controlled drug release, Carbohydr. Polym. 214 (2019) 8–14.
[42] S. Yadav, I. Ibrar, A. Altaee, A.K. Samal, J. Zhou, Surface modification of nanofiltration membrane with kappa-carrageenan/graphene oxide for leachate wastewater treatment, J. Membr. Sci. 659 (2022) 120776.
[43] J. Yang, Y. Chen, L. Zhao, J. Zhang, H. Luo, Constructions and properties of physically cross-linked hydrogels based on natural polymers, Polym. Rev. 63 (3) (2023) 574–612.
[44] P. Yang, F. Yu, Z. Yang, X. Zhang, J. Ma, Graphene oxide modified κ-carrageenan/sodium alginate double-network hydrogel for effective adsorption of antibiotics in a batch and fixed-bed column system, Sci. Total Environ. 837 (2022) 155662.
[45] N.L. Yue, M.C. Jennings, R.J. Puddephatt, Dimerization of an organoplatinum complex triggered by oxidative addition: a model for dynamic ring-opening polymerization, J. Organomet. Chem. 803 (2016) 45–50.
[46] T. Zhang, S. Xiao, K. Fan, H. He, Z. Qin, Preparation and adsorption properties of green cellulose-based composite aerogel with selective adsorption of methylene blue, Polymer 258 (2022) 125320.